



Transport and retention of colloidal particles in partially saturated porous media: Effect of ionic strength

Yuniati Zevi,¹ Annette Dathe,¹ Bin Gao,^{1,2} Wei Zhang,¹ Brian K. Richards,¹ and Tammo S. Steenhuis¹

Received 30 July 2008; revised 23 July 2009; accepted 28 August 2009; published 4 December 2009.

[1] We directly observed pore-scale attachment of fluorescent synthetic polystyrene colloids (1.0 μm diameter) in a partially saturated sand pack (pore space saturation ranging from 0.7 to 0.9) at four solution ionic strengths (0, 1, 100, 200 mmol NaCl). Sequential confocal laser microscope images were analyzed to quantify colloid retention, particularly at air-water meniscus-solid (AW_{mS}) interfaces. We concurrently measured effluent colloid concentrations to determine overall matrix retention. Ionic strength had no effect on meniscus contact angles (26.7 ± 3.7 degrees) or surface tension (63–67 mN/m), both important components of the capillary forces thought to play the primary role in retention at the AW_{mS} interfaces. AW_{mS} interfaces attachment was greatest at 1 mmol, with the 0 mmol ionic strength reducing attachment by half. Increasing ionic strength to 100 and 200 mmol markedly decreased colloid retention at the AW_{mS} interfaces due to observed increased competing attachment at grain surfaces (solid/water interface) that reduced the number of colloids available for AW_{mS} interface attachment.

Citation: Zevi, Y., A. Dathe, B. Gao, W. Zhang, B. K. Richards, and T. S. Steenhuis (2009), Transport and retention of colloidal particles in partially saturated porous media: Effect of ionic strength, *Water Resour. Res.*, 45, W12403, doi:10.1029/2008WR007322.

1. Introduction

[2] Colloid-facilitated transport, which has received considerable attention in recent years, can significantly enhance the movement of contaminants to groundwater in both saturated and unsaturated soils [Ouyang *et al.*, 1996; Schäfer *et al.*, 1998a; Kretzschmar and Sticher, 1998; Sen and Khilar, 2006]. The vadose (or unsaturated) zone of soil profiles plays an important buffering role in mitigating contaminant transport to groundwater, but our understanding of colloid retention and remobilization in this zone is far more limited than the better understood mechanisms in saturated groundwater zones [Weisbrod *et al.*, 2003].

[3] Findings of colloid transport and retention have been primarily based on laboratory column breakthrough curves which are limited in that they represent the aggregate effect of all processes occurring in the test column and cannot uniquely identify the various mechanisms of colloid retention or mobilization. However, direct pore-scale visualization is a promising approach that can help discern specific mechanisms, but relatively few unsaturated visualization experiments have been conducted to date. Using pore micromodels, Wan and Wilson [1994a] and Sirivithayapakorn and Keller [2003] concluded that colloids were retained at the air-water (AW) interface, but Chen and Flury [2005] did not observe interception and attachment of mineral colloids at the AW interface. Gao

et al. [2006] found that colloids were retained both by straining in thin water films around sand grains and by trapping in immobile water zones, with subsequent pendular ring expansion causing sudden rerelease of colloids. Using 3-D sand flow chambers, Crist *et al.* [2004, 2005] and Zevi *et al.* [2005, 2006] found that colloids were primarily retained at the locations where water menisci connecting sand grains diminish to thin water films, and termed this region as the air-water meniscus-solid (AW_{mS}) interface.

[4] The mechanisms of colloid retention at the AW_{mS} interface are not well known. The classic Derjaguin-Landau-Verwey-Overbeek (DLVO) theory [e.g., Schäfer *et al.*, 1998b; Sirivithayapakorn and Keller, 2003; Auset and Keller, 2006; Lazouskaya *et al.*, 2006], cannot explain the retention of anionic hydrophilic colloids at the AW_{mS} interface [Crist *et al.*, 2005], suggesting that there must be additional forces retaining colloids at this interface. Several authors [Sirivithayapakorn and Keller, 2003; Wan and Wilson, 1994b; Zevi *et al.*, 2005] have proposed capillary forces to explain colloid attachment at AW interfaces as well as straining in thin water films [Gao *et al.*, 2006; Wan and Tokunaga, 1997], mainly because capillary force energy potentials can be several orders of magnitude greater than those calculated with DLVO forces [Jewett *et al.*, 1995; Kralchevsky *et al.*, 2001; Kralchevsky and Nagayama, 2000; Sur and Pak, 2001; Gao *et al.*, 2008]. Most studies of unsaturated colloid transport have quantified the forces on colloidal particles at interfaces, liquid films and biomembranes under static conditions [Kralchevsky *et al.*, 2001; Gao *et al.*, 2008; Lazouskaya *et al.*, 2006; Lazouskaya and Jin, 2008; Kralchevsky and Nagayama, 2000]. Recently Gao *et al.* [2008] and Shang *et al.* [2008] investigated how capillary and DLVO forces at the AW_{mS} interface affect colloid

¹Department of Biological and Environmental Engineering, Cornell University, Ithaca, New York, USA.

²Now at Department of Agricultural and Biological Engineering, University of Florida, Gainesville, Florida, USA.

retention in unsaturated porous media. Although slightly different approaches were used in these studies, the capillary forces were two orders of magnitude greater than the DLVO forces. In addition, *Shang et al.* [2008] determined that capillary forces were greater than hydrodynamic forces. More recently, *Shang et al.* [2009] found that capillary forces exerted by moving air/water interfaces exceed DLVO forces and can detach stationary particles.

[5] Capillary forces at the AW_mS interface are exerted on colloids deforming the meniscus surface film [*Gao et al.*, 2008]. The total capillary force can be decomposed into a normal force acting perpendicular to the grain surface and a lateral force acting parallel to the grain surface. The normal force component generates the friction force that acts to retain the colloid at the interface. Conversely, when the lateral capillary force exceeds the friction force (or when there is no friction force such as when the water film is thicker than the colloid diameter [*Sur and Pak*, 2001]), the colloid is pushed back into the bulk solution. *Gao et al.* [2008] further argued that fewer colloids would be retained at AW_mS interfaces on smooth grain surfaces as compared to rougher surfaces, which was subsequently confirmed by *Morales et al.* [2009].

[6] The effect of changing solution ionic strength on colloid retention at the AW_mS interface is unknown. Increasing ionic strength lessens the magnitude of the energy barrier (as calculated by DLVO forces), and leads to progressively more favorable conditions for colloid retention on solid surfaces in saturated systems [*Compere et al.*, 2001] and at air-water interfaces in unsaturated systems [*Saiers and Lenhart*, 2003]. Breakthrough studies have shown that increasing ionic strength generally increases colloid retention [*Jewett et al.*, 1995; *Li and Logan*, 1999; *Compere et al.*, 2001; *Saiers and Lenhart*, 2003]. It is possible that changes in ionic strength could alter the nature and magnitude of capillary interfacial interaction energies by changing the surface tension (σ), although the effect is likely small at typical environmental levels [*Poling et al.*, 2001; *Li et al.*, 1999] and/or contact angles (θ) between the water phase and solid surfaces. *Li et al.* [1999] calculated that NaCl concentrations up to 1 molal slightly increased surface tension to 74 mN/m.

[7] The goal of these experiments was to thus to define the effects of increasing ionic strength on colloidal attachment at the AW_mS interface. Our objectives were to (1) use pore-scale confocal microscope visualization to directly observe and quantify changes in colloidal AW_mS interface attachment in a partially saturated sand chamber at different solution ionic strengths (0, 1, 100, and 200 mmol NaCl) and (2) use concurrent breakthrough curve determinations to measure trends in overall matrix colloid retention for comparison with visualization measurements.

2. Material and Methods

2.1. Experimental System

[8] Synthetic polystyrene microspheres (1.0 μm diameter; Magsphere Inc, Pasadena, California) were used as experimental colloids because of their high confocal microscope signal intensity. Colloid input concentrations were 1.8×10^8 particles/mL, with the pH of the colloid suspension adjusted to 5.7 with dilute HCl/NaOH additions. Sus-

pensions were prepared by diluting the concentrated stock suspension 1:1250 with NaCl solution to achieve ionic strengths of 0, 1, 100 and 200 mmol. Rhodamine B was added at less than 2.1×10^{-5} M (a concentration expected to reduce pure water surface tension by less than 0.6%, interpolating from *Ghosh and Nath* [1932] to allow imaging of the water phase. Although subsequent results showed no effect on attachment behavior, a portion of our experiments used colloids that were prewashed by centrifuging the stock suspension, decanting, and resuspending in deionized (DI) water as described by *Bangs and Merza* [1995]. This was done to remove the unspecified surfactant added by the colloid manufacturer to the stock suspension (0.01% w/w concentration). In any case, the concentration of surfactant from unwashed colloids in the diluted flow solutions would have been negligible at approximately 0.08 ppm.

[9] The porous medium used was 0.4–0.6 mm diameter quartz sand (Unimin Corp.), acid washed (HNO_3) and rinsed with deionized water as per *Lenhart and Saiers* [2002]. The average porosity of the sand pack was 0.354 ± 0.026 cm^3/cm^3 as determined from the bulk density ($\rho_b = 1.70$ g/cm^3) and sand particle density ($\rho_s = 2.65$ g/cm^3).

[10] The schematic of the experimental apparatus (explained in greater detail by *Zevi et al.* [2006]) is shown in Figure 1. An acrylic flow chamber (10 mm \times 30 mm \times 3 mm; capacity of 1.6 g sand) was fitted with porous ceramic plates (40–60 μm pore size; R&H Filter Co. RH-1000) at the inlet and outlet to assure unsaturated flow conditions. Two syringe pumps supplied water and colloid suspension at the inlet, and a peristaltic pump removed the flow from the outlet. The injection assembly consisted of syringes I and II, inlet tubing components (designated A, B, and C), and one Y fitting. Tubing A and B (inside diameter 1.14 mm) linked the syringes to the Y fitting, while C connected the fitting to the chamber inlet. The total length of inlet tubing (either A + C or B + C) was 31 cm. Syringe I was filled with background solution (adjusted to target ionic strength and pH), and Syringe II was filled with the tracer or colloid suspension.

[11] Background solution was pumped from Syringe I until the porous medium was fully saturated. The effluent pump was then activated to desaturate the porous media. The effluent flow rate was measured until the inflow and outflow equilibrated at approximately 0.1 mL/min. Syringe I was then stopped as the second syringe pump began to inject the Syringe II solution (either tracer or colloid) into the column through tubing B + C. The time when the tracer or colloid solution reached the porous plate was established as $t = 0$. After the completion of Syringe II, the injection of background solution was resumed.

2.2. Experimental Methods

[12] In addition to direct observation detailed below, colloid and tracer breakthrough experiments were performed by sampling effluent colloid concentrations at 2 min intervals, with samples diluted with known volumes of distilled water for subsequent analysis. Breakthrough experiments were performed in duplicate; some were performed without taking simultaneous confocal images. Breakthrough curves with no sand pack in place were run to determine system (i.e., chamber/plate/tubing) colloid retention. Bromide breakthrough experiments were also performed (25 mg Br/L input solution) to determine the

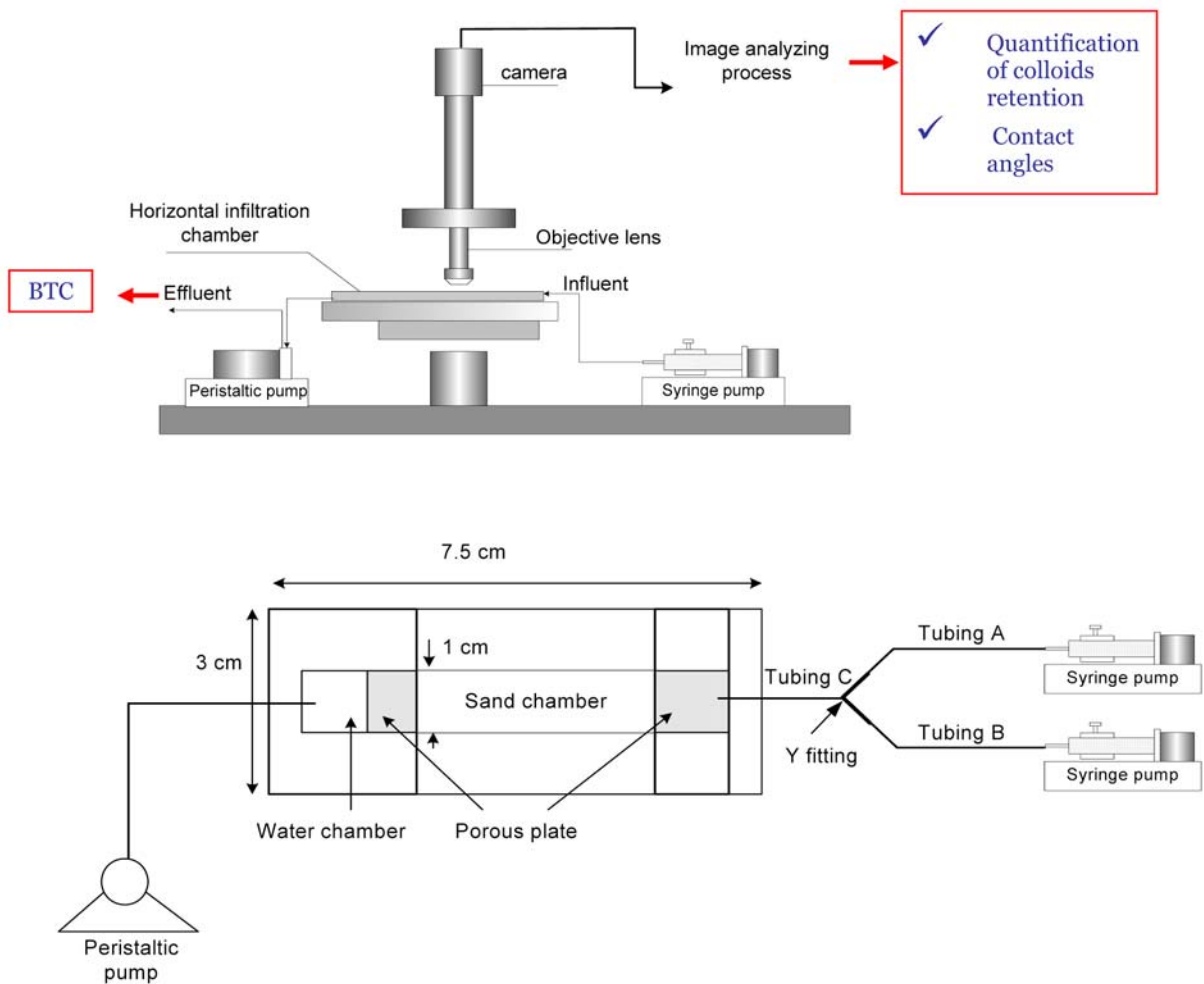


Figure 1. Schematic of experimental apparatus.

interstitial velocity and dispersivity of the water in the sand pack using the convective-dispersion equation as implemented in the CXTFIT2 program. Effluent colloid concentrations were analyzed by measuring fluorescence at excitation and emission wavelengths of 485 nm and 538 nm respectively, using a Fluoroskan Ascent FL 2.5 fluorimeter. Effluent bromide concentrations were analyzed using a Dionex ICS 2000 ion chromatography system with an IonPac AS18 column.

[13] Breakthrough curves of colloids were adjusted for travel time and the retention of the colloids in the porous plates and tubing. In order to determine final mass balances, colloids sorbed onto the sand pack and those retained in the apparatus apart from the sand pack were quantified. At the end of each test, the sand pack was removed from the chamber for moisture content analysis. The sand was then placed in 1 mL distilled deionized (DDI) water and sonicated for 10 min, with the resulting aliquot analyzed for colloid (or Br) content. Colloids remaining in the tubing and porous plates were rinsed out with a known volume of distilled water and measured. Experiments with tubing and an empty chamber showed that the system had a consistent loss of 3.5% of injected colloids, an amount that agreed with the amount recovered after back flushing. With these

results, the mass balances and breakthrough calculations were normalized to represent only the colloids that entered the chamber and were either recovered in the effluent or retained on the sand. Colloid travel times were consistently 20 s through the porous plate and 4.7 min through the outlet tube, with little variance among the four replicates. Breakthrough times were therefore adjusted by these quantities to obtain the true sand pack travel times.

[14] Surface tension measurements were made in triplicate at 25°C with a Model 21 Surface Tensiomat (Fisher Scientific, Pittsburgh, Pennsylvania) fitted with a 19 mm diameter platinum-iridium ring. Solutions were placed in a 50 mm diameter shallow glass dish and the ring was inserted in the middle of the dish to avoid edge effects. The ring was raised through semiannual operation of the torsion mechanism, and the tension reading at the instant of surface detachment was noted.

[15] The zeta potential of the sand was estimated from measurements made on colloidal-sized sand fragments as per *Saiers and Lenhart* [2003], with fragments obtained by sonicating sand submerged in DI water for 30 min. The resulting aliquots were filtered (0.45 μm membrane filter) and adjusted to match experimental ionic strengths with NaCl additions prior to measurement. The zeta potential

Table 1. Experimental Conditions for Each Experiment Using Synthetic 1.0 μm Polystyrene Colloids

Experiment Number	Colloids Prewashed?	Ionic Strength (mmol)	Resolution ($\mu\text{m}/\text{pixel}$)	Image Size (pixels)	Threshold Level	Time Step (s)	Replicates	Regions per Replicates	Total Sequences.	Frames per Sequence	Total Elapsed Time (min)	Breakthrough Curve Replicates
1	Y	1	0.73	1024 \times 1024	100	2.0	2	2	8	121	39	
2	Y	100	0.37	1024 \times 512	50	1.0	3	2	4	242(3), 121(1)	36	
3	Y	200	0.37	1024 \times 1024	50	1.5						
				1024 \times 1024	38	1.5	2	2		61(8), 121(5), 61(1)	19,22	
4	N	0	0.37	1024 \times 1024	110	1.5	1	2	7	61	15	2
5	N	1	0.37	1024 \times 1024	110	1.5	2	2	6	96(1), 121(5)	31	2
6	N	100	0.37	1024 \times 1024	100	1.5	3	2	6	121	30	2
7	N	200	0.37	1024 \times 1024	90	1.5	2	2	6	121	26	2

was determined with a Lazer Zee Model 501 m (PenKem, Bedford Hills, New York). *Johnson* [1999] found good agreement when comparing a similar microfragment approach with streaming zeta potential determinations for sand.

2.3. Pore-Scale Imaging and Analysis

[16] The visualization system was a Leica TCS SP2laser scanning confocal microscope with HC PL APO CS 10.0X objectives with a numerical aperture of 0.4, yielding a resolving power of 0.37 μm . The system can record either a time series of images at one plane or 3-D representations composed of images taken at 1 μm depth intervals. The microscope obtained separate images of the colloids, water, and grains using three spectral channels. In the first channel, emissions from the fluorescent colloids excited at 488 nm (argon laser) were recorded in the range of 500 to 540 nm. In the second channel, the water phase stained with Rhodamine B was excited at 543 nm (green HeNe laser) with the emission recorded in the range of 555 to 650 nm. The third channel detected transmitted light to show the location of the sand grains. These three channels were acquired as 8 bit gray scale images, with the argon and HeNe channels displaying the fluorescence in false-colored yellow-green and red, respectively.

[17] For quantification purposes, the image analysis procedure developed by *Zevi et al.* [2006] was used for counting colloids in image stacks acquired using ImageJ software (National Institutes of Health, <http://rsb.info.nih.gov/nih-image/>). The procedure consisted of transforming the confocal microscope images to black and white (binary) images by thresholding the argon channel images (of colloid locations), and separating pixels in order to identify them as either colloid or background. In the thresholding process, gray values recorded by the argon channel ranging from 0 (black) to 256 (white) were separated by a specified threshold gray value. The threshold value was chosen empirically such that the outline of colloids in thresholded images appeared the same as in the original images. No further image enhancement took place except where interference was encountered from false light reflecting from the water surface.

[18] After thresholding, the regions with colloid retention near observed AW_{mS} interfaces were selected. The regions were applied to all the sequential images in a stack, thus allowing automatic counting. The Boolean “and” operator was used to compare sequential images, detecting all colloid pixels which appeared at exactly the same position (and thus could be judged as retained). Pixels were counted as colloids when two or more pixels were connected using the eight neighborhood method. The total area of colloids was then calculated as the product of the number of pixels and the pixel size. A simple macro was used to automate the counting process. Colloid concentrations were expressed as area of colloids per unit interface length ($\mu\text{m}^2/\mu\text{m}$).

[19] The imaging resolution, image size, imaging threshold, number of sequences, regions, frames per sequence and total elapsed time are summarized in Table 1.

2.4. Contact Angle Measurement

[20] Contact angle measurements were obtained using reconstructed images sectioned in succession along the z axis such as those shown in Figures 2b and 2c. From these

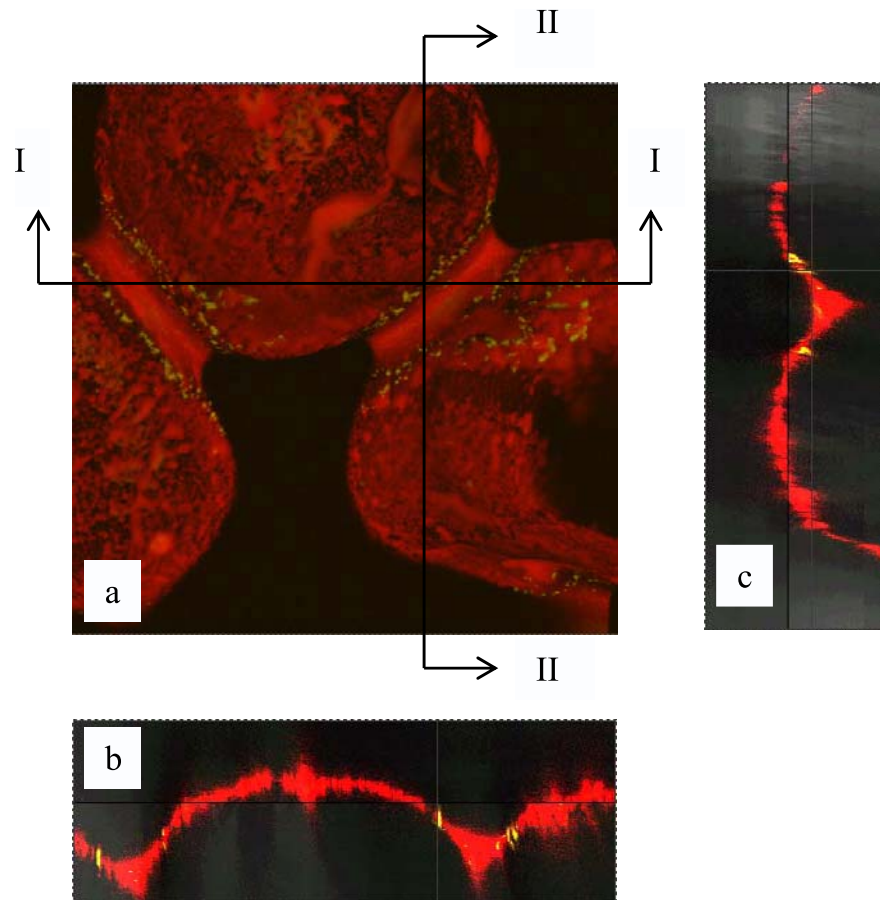


Figure 2. An example of overlaid confocal microscope image: (a) Top view of three sand grains joined by pendent rings of water, with notable attachment of colloids (light) at AW_mS interfaces. (image size $795 \times 795 \mu\text{m}$), (b) cross-section image taken along Plane I: cross section of water film covering sand grain, thickening at pendent rings, with colloid attachment at AW_mS interfaces (image size $795 \times 272 \mu\text{m}$) and (c) similar cross section along section II (image size $795 \times 272 \mu\text{m}$).

images we determined the angle of tangent line to the grain and meniscus (derivation shown in the auxiliary material).¹ The difference between the two angles of the tangent lines was the contact angle. The measurements were repeated for ten different cross sections because of variation observed between individual measurements.

3. Results

[21] Volumetric sand pack water contents determined gravimetrically at the conclusion of experiments were $0.25\text{--}0.26 \text{ g/cm}^3$ (influent end) and $0.30\text{--}0.33 \text{ g/cm}^3$ (effluent end) of the sand pack, corresponding to pore saturation extents of $0.70\text{--}0.74$ and $0.85\text{--}0.94$, respectively. There were no significant differences in either zeta potential or surface tension from washed versus unwashed colloids, so the values shown in Table 2 show the mean of all measurements of both washed and unwashed colloids. The zeta potential of colloids increased from -62.4 mV to -22.6 mV as the ionic strength increased from 0 to 200 mmol. Similarly, the zeta potential for sand increased from -51.8 mV at 0 mmol ionic strength to -11.5 mV

for 200 mmol. The increasing solution NaCl concentration appeared to slightly increase surface tension from 63.2 to 66.8 mN/m, although the variability among several replicates was substantial enough to prevent this increase from being significant.

[22] The retention of the colloids was observed by measuring both the effluent colloid concentration and by pore scale imaging. Colloid attachment at the pore scale is shown as still images, videos, and is summarized as plots of cumulative colloid attachment over time. For each treatment, either one or two sets of experiments were conducted at pores where colloid retention could be

Table 2. Measurement of Zeta Potential, Solution Surface Tension, and Measured Water Meniscus-Grain Contact Angles^a

Solution Ionic Strength (mmol)	Zeta Potential (mV)		Surface Tension
	Colloid	Sand	σ (mN/m)
0	-62.4 ± 3.4	-51.8 ± 2.1	63.2 ± 0.8
1	-47.3 ± 2.3	-41.2 ± 2.8	64.5 ± 1.1
100	-27.6 ± 2.5	-19.6 ± 3.2	66.6 ± 0.2
200	-22.6 ± 2.2	-11.5 ± 2.9	66.8 ± 5.0

¹Auxiliary materials are available in the HTML. doi:10.1029/2008WR007322.

^aZeta potential is estimated from colloids and sand fragments.

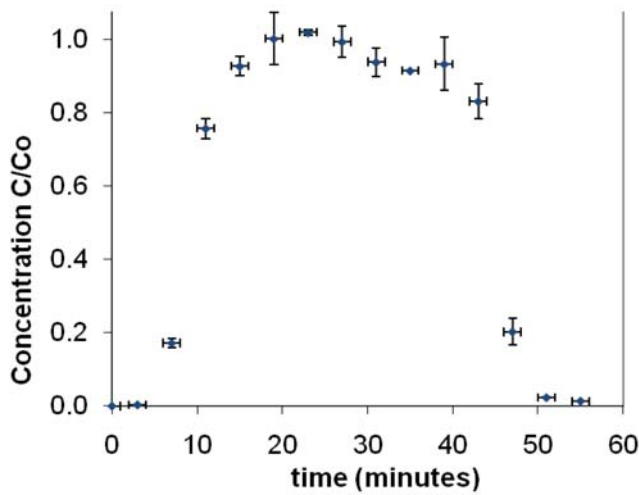


Figure 3. Mean and standard deviation of replicate bromide tracer breakthrough curves. The x axis error bars represent slight variation in sampling time between replicate runs.

clearly observed. In addition to still images, the pore movement of colloids was recorded as video sequences which are available as auxiliary material.

3.1. Breakthrough Curves

[23] Breakthrough curves represent an aggregated response of the various mechanisms affecting colloid reten-

tion in the sand column. In general, breakthrough curves for both the Br tracer (Figure 3) and colloids (Figure 4) consisted of an initial zero effluent concentration phase, a rapid increase phase to the peak level, and then a tailing phase after the colloid pulse ended and background solution was resumed. The maximum breakthrough concentration for colloids was consistently lower than that for nonadsorbed bromide, indicating retention of colloids in the sand column.

[24] The initial breakthrough of colloids and bromide occurred simultaneously approximately 3 min after injection, consistent with an expected velocity of 1.0 cm/min based on a flux of 0.1 mL/min, chamber length of 30 mm, chamber cross section of 10 mm \times 3 mm, and a volumetric water content of 0.35. Tracer breakthrough analysis shows that the average pore water velocity in the sand pack was 1.0 cm/min, and the dispersion coefficient was 0.065 cm²/min.

[25] Colloid breakthrough curves (Figure 4) indicated that increasing ionic strength resulted in increased colloidal retention within the porous sand medium (Table 3). This trend was best defined when comparing the 0 and 200 mmol treatments. The reason for the increased variance between replicate runs at 1 and 100 mmol ionic strengths is not known. Comparison of fractional effluent recovery of colloids (Table 3) showed a similar trend, with the variation among replicates greatest for 1 and 100 mmol ionic strengths but a significant ($P < 0.05$) difference only between the 0 versus 200 mmol treatments.

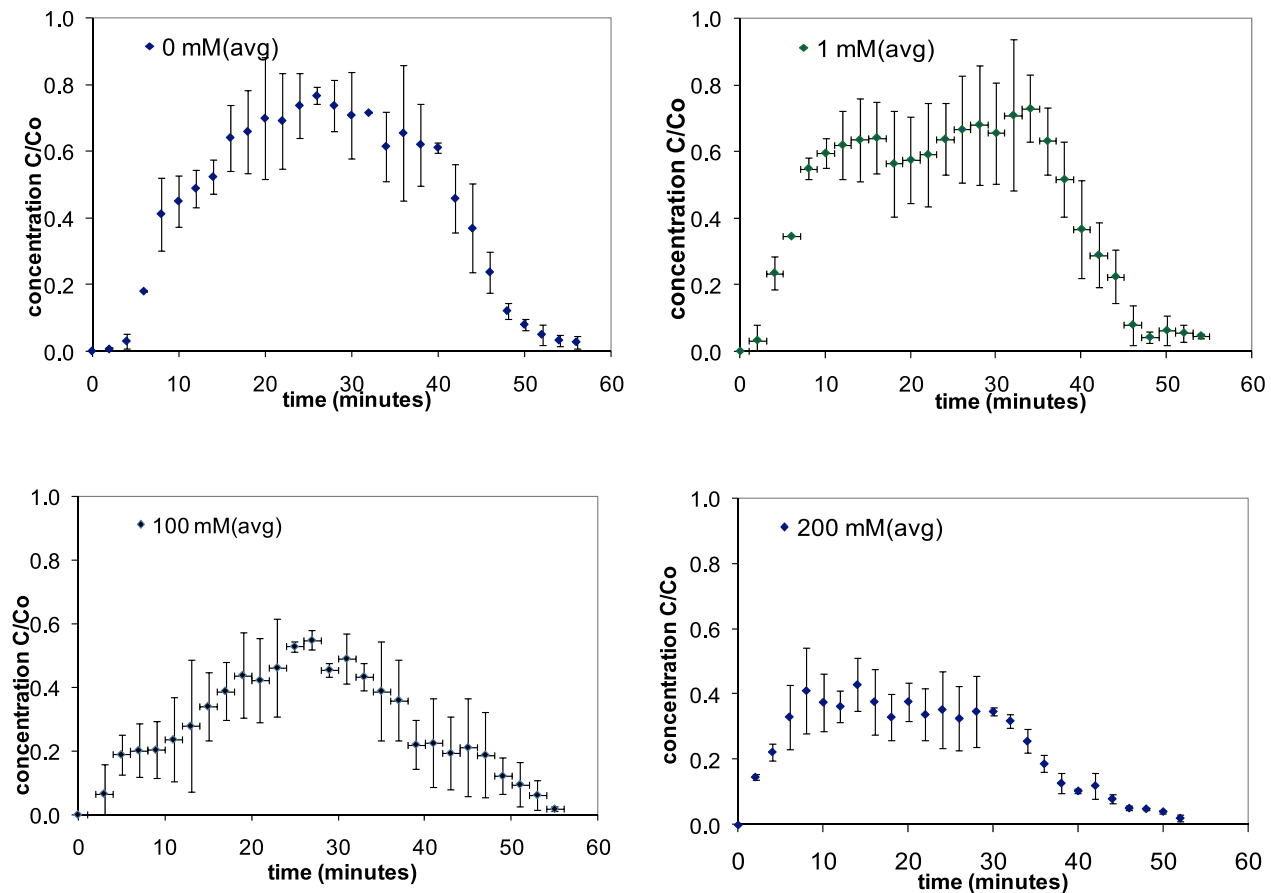


Figure 4. Breakthrough curves for polystyrene colloids at differing ionic strengths.

Table 3. Fractional Effluent Colloid Recovery From Colloid Breakthrough Curves^a

Solution Ionic Strength (mmol)	Fraction Recovered
0	0.82 ± 0.08
1	0.79 ± 0.14
100	0.52 ± 0.14
200	0.43 ± 0.04

^aColloid breakthrough curves are estimated from unwashed colloids. Mass balance was adjusted for the 3.5% of input concentration retained by empty chamber.

3.2. Pore-Scale Imaging

[26] Pore-scale images and video sequences are presented in the auxiliary material. The mean water meniscus/grain contact angle measured from 10 cross-sectional images at each ionic strength was 26.7 ± 3.7 degrees, with no observable effect of ionic strength or colloid prewashing (Table 4). Time series plots of the areas of attached colloids at AW_{mS} interfaces calculated via image analysis are presented in Figure 5 for experiment series 1 to 7. Each plot represents mean values from replicate series, and $t = 0$ represents the arrival of the first observed colloid at the specified location. Interruptions in imaging due to the saving file process varied for every series and led to the observed data breaks. In general, colloid retention at the AW_{mS} interface decreased as ionic strength increased, with results similar for both washed and unwashed colloids and thus aggregated here. The maximum retention of colloids at observed AW_{mS} interfaces was greatest at ionic strengths of 1 mmol, with end-of-sequence values of 1.6 to $2 \mu\text{m}^2/\mu\text{m}$ for series 2 and 5. Cumulative retention at the same time point for 0 mmol ionic strength was somewhat lower at circa $0.75 \mu\text{m}^2/\mu\text{m}$. The 100 mmol experiments had cumulative attachment extents of approximately $0.2 \mu\text{m}^2/\mu\text{m}$ (series 3 and 6), while 200 mmol ionic strengths had the lowest cumulative attachment levels of 0.05 to $0.07 \mu\text{m}^2/\mu\text{m}$ for series 4 and 7.

4. Discussion

[27] Each of the two approaches for quantifying retention used offers advantages and limitations. The limited working distance under the confocal microscope objective required a thin chamber in which small changes in packing could result in relatively large changes in breakthrough, which may have contributed to the variation seen with some

Table 4. Measured Sand Grain-Water Meniscus Contact Angle Summary for Solutions Containing Both Unwashed and Washed Colloids

Solution Ionic Strength (mmol)	Contact Angles ^a (deg)	
	Unwashed Colloids	Washed Colloids
0	27.7 ± 4.3	NA ^b
1	23.8 ± 2.5	24.5 ± 5.5
100	28.3 ± 2.7	26.2 ± 1.9
200	28.3 ± 3.8	28.4 ± 1.5

^aThe mean for unwashed and washed colloids is 26.7 ± 3.7 .

^bNA means not available.

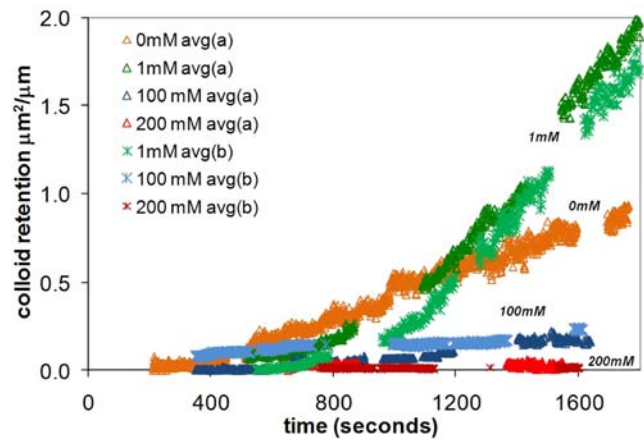


Figure 5. Time series of colloid retention ($\mu\text{m}^2/\mu\text{m}$) at the AW_{mS} interface measured from confocal microscope image sequences. Each plot series represents the mean of replicate time series experiments. Legend suffix *a* represents unwashed colloids and *b* washed colloids. Solution ionic strengths of 0 mmol (series 4, orange), 1 mmol (series 1, light green and 5, dark green), 100 mmol (series 2, light blue and 6 dark blue) and 200 mmol (series 3 dark red and 7 medium red).

treatments. On the other hand, while visualization gives powerful pore-scale insights, we are able to visualize only a limited number of interfaces and thus the absolute magnitude of our pore-scale AW_{mS} retention determinations could differ from the true overall extent. However, the general trends determined by pore scale observations versus breakthrough experiments should be valid.

[28] Increasing ionic strength affected neither the contact angle which remained at 25 degrees nor the surface tension of approximately 65 mN/m, and thus the magnitude of the capillary forces primarily responsible for attachment at the AW_{mS} interface would have been minimally affected by changes in ionic strength. Nevertheless, the retention of colloids at the AW_{mS} interface decreased dramatically with increasing ionic strength from 1 to 100–200 mmol (Figure 5). The somewhat lower attachment extent observed at 0 mmol ionic strength was surprising, but may be related to how we hypothesize that colloids get to the AW_{mS} interface in the first place. Bradford *et al.* [2007, 2009], Bradford and Torkzaban [2008] and others [Torkzaban *et al.*, 2007, 2008; Tong *et al.*, 2008] held that colloids roll and slide on the grain surface and are funneled by hydrodynamic drag forces into wedge-shaped grain-grain contact points in saturated porous media. It is possible that the same idea may hold true for movement of colloids toward the similarly shaped AW_{mS} interface in unsaturated conditions. Since 0 mmol ionic strength is extremely dilute and minimal colloids will attach to grain surface (as per the DLVO energetics diagram in Figure 6; calculation approach elaborated in the auxiliary material), there may not be enough colloids close to the grain surface to be funneled into the AW_{mS} . When ionic strength increases slightly (1 mmol case), more colloids would present near the surface and available to be funneled to the AW_{mS} interface. However, further increases in ionic strength would cause the adhesive forces between colloids and grains prevail, reducing the amount of

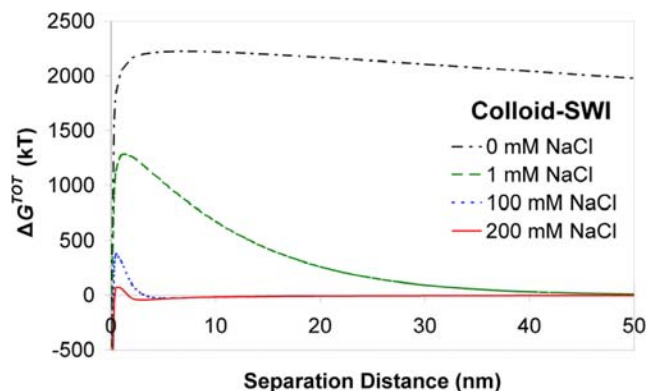


Figure 6. Total DLVO interaction energy (ΔG^{TOT}) of polystyrene colloids interacting with the sand-water interface (SWI) in 0 mmol, 1 mmol, 100 mmol, and 200 mmol NaCl solutions.

colloids that can be funneled to AW_mS by hydrodynamic drag. There may thus be a nonlinear effect of ionic strength on attachment at the AW_mS interface.

[29] In contrast to the patterns seen at the AW_mS interface, the breakthrough curves suggested increasing colloid retention with increasing ionic strength, consistent with numerous literature findings of increased ionic strength reducing the magnitude of the energy barrier near the solid surface, thus inducing more favorable conditions for colloid attachment at the grain surface. Calculations of DLVO interfacial energies using measured sand and colloid properties (summarized in Figure 6) indicate significant lessening of repulsions at higher ionic strengths, which would facilitate increased attachment throughout the matrix.

[30] Given these apparently conflicting findings of decreased retention at the AW_mS interface but increased overall matrix retention, we examined the composed 3-D images taken at circa 1200 s into the experiments. Unlike

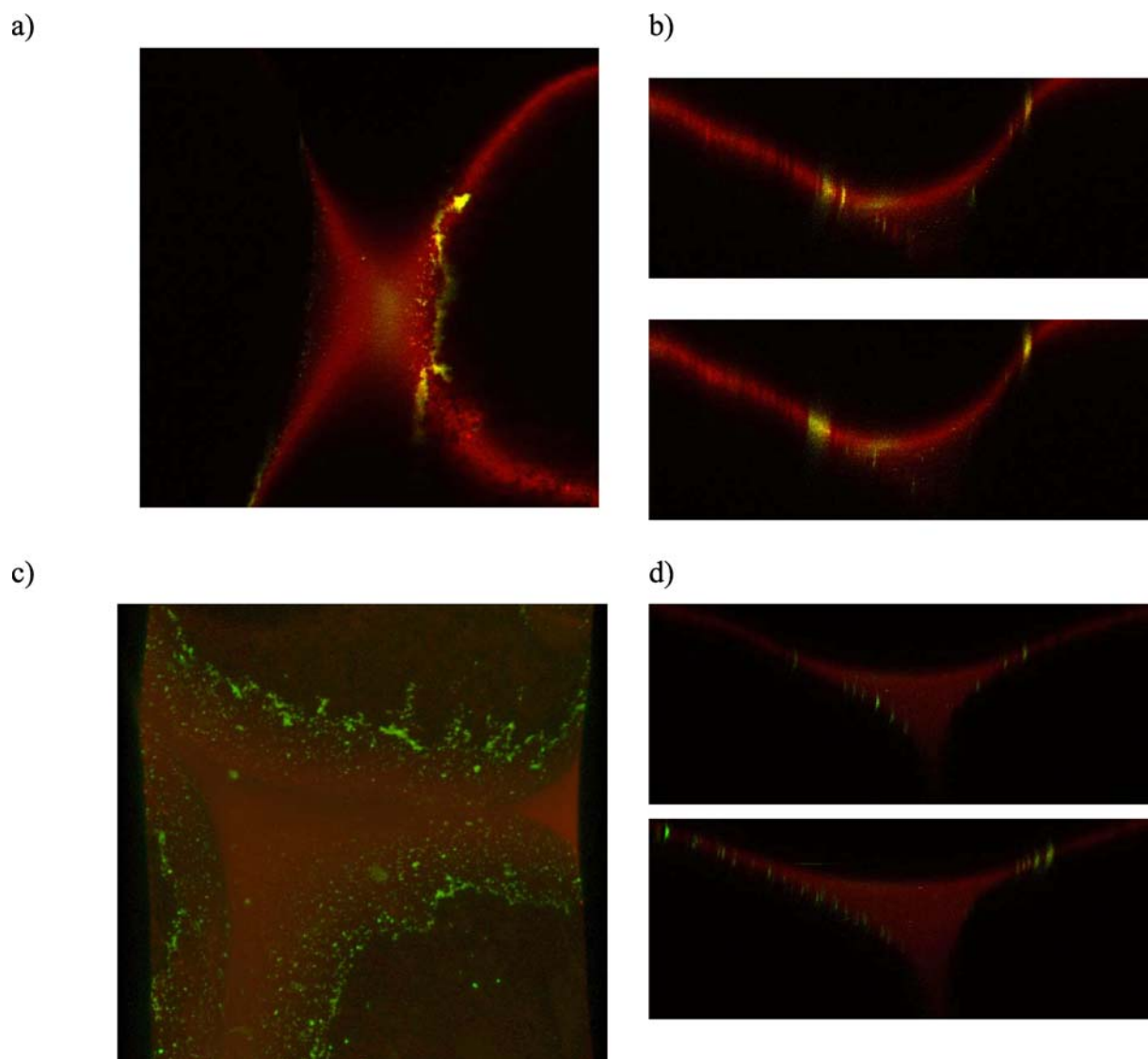


Figure 7. Effect of ionic strength on colloids retention at the AW_mS and solid-water interfaces: (a) at 1 mmol, colloid retention (light) concentrated at AW_mS of meniscus (red) between two sand grains on left and right sides of image; (b) cross section of interface showing similar concentration at interface; (c) at 100 mmol, colloid retention visible scattered across the submerged sand grain surfaces; and (d) meniscus cross section similarly showing colloid distribution across grain surfaces.

the images used for quantification of the retention of colloids at the AW_mS interface, the 3-D images enable the viewer to see other focal planes, including the solid-water interface. The 3-D figures showed that at low ionic strengths, colloids were essentially only attached at the AW_mS interface (Figures 7a and 7b, 1 mmol). In contrast, at higher ionic strengths, the colloids were retained at much greater amounts across the submerged grain surfaces (i.e., at the solid-water (SW) interface), and to a much lesser extent at the AW_mS interface (Figure 7c, 100 mmol). Similarly, the meniscus cross section in Figure 7d shows colloid distribution across grain surfaces at 100 mmol ionic strength. As such, it is likely that colloid retention at the AW_mS interface decreased under increasing ionic strength conditions because of increased competition from grain surface retention sites whose retention energetics became more favorable and whose relative areas available for attachment were much greater. Thus ionic strength affected the extent of retention at the AW_mS indirectly by reducing the number of colloids available to preferentially attach to that interface.

[31] It is important to note that our results differ from Lazouskaya *et al.* [2006] who found no effect of increasing ionic strength at the AW_mS interface in the microchannel used for their study. However, in their case, there was no competitive retention of colloids by the WS interface in the smooth glass channel; the disparity in surface roughnesses of the respective medium surfaces may have contributed to the divergence of results between their study and ours. Indeed, examination of Figure 7c suggests that colloid distribution on the grain surface in our study was not uniform but clustered, which suggests that grain surface irregularities and roughness may be an important physical property influencing colloid retention [Morales *et al.*, 2009].

5. Conclusions

[32] Direct visual quantification showed that increasing ionic strength reduced retention at the AW_mS interface by increasing the favorability of competing attachment at submerged grain surfaces (solid-water interfaces) and thus reducing the number of colloids available to approach and attach at the AW_mS interface. This observation of tradeoffs between differing interfaces illustrates the advantage of direct visual quantification over inferential observations such as breakthrough curves.

[33] **Acknowledgments.** This research was supported by funding from the USDA-National Research Initiative (project 2005-03929) and the National Science Foundation (project 2006-0635954). The authors acknowledge the expert guidance of Carol Bayles, manager of the Cornell University Biotechnology Center's Microscopy and Imaging Facility.

References

- Auset, M., and A. A. Keller (2006), Pore-scale visualization of colloid straining and filtration in saturated porous media using micromodels, *Water Resour. Res.*, *42*, W12S02, doi:10.1029/2005WR004639.
- Bangs, L. B., and M. Merza (1995), Microspheres, part 1: Selection, cleaning, and characterization, *IVD Technol. Mag.*, March, 8–10.
- Bradford, S. A., and S. Torkzaban (2008), Colloid transport and retention in unsaturated porous media: A review of interface, collector, and pore scale processes and models, *Vadose Zone J.*, *7*, 667–681, doi:10.2136/vzj2007.0092.
- Bradford, S. A., S. Torkzaban, and S. L. Walker (2007), Coupling of physical and chemical mechanisms of colloid straining in saturated porous media, *Water Res.*, *41*, 3012–3024.
- Bradford, S. A., S. Torkzaban, F. Leij, J. Šimůnek, and M. T. van Genuchten (2009), Modeling the coupled effects of pore space geometry and velocity on colloid transport and retention, *Water Resour. Res.*, *45*, W02414, doi:10.1029/2008WR007096.
- Chen, G., and M. Flury (2005), Retention of mineral colloids in unsaturated porous media as related to their surface properties, *Colloids Surf. A*, *256*(2–3), 207–216, doi:10.1016/j.colsurfa.2005.01.021.
- Compere, F., G. Porel, and F. Delay (2001), Transport and retention of clay particles in saturated porous media. Influence of ionic strength and pore velocity, *J. Contam. Hydrol.*, *49*, 1–21, doi:10.1016/S0169-7722(00)00184-4.
- Crist, J. T., J. F. McCarthy, Y. Zevi, P. C. Baveye, J. A. Troop, and T. S. Steenhuis (2004), Pore-scale visualization of colloid transport and retention in partly saturated porous media, *Vadose Zone J.*, *3*(2), 444–450, doi:10.2113/3.2.444.
- Crist, J. T., Y. Zevi, J. F. McCarthy, J. A. Troop, and T. S. Steenhuis (2005), Transport and retention mechanisms of colloids in partially saturated porous media, *Vadose Zone J.*, *4*, 184–195.
- Gao, B., J. E. Saiers, and J. Ryan (2006), Pore-scale mechanisms of colloid deposition and mobilization during steady and transient flow through unsaturated granular media, *Water Resour. Res.*, *42*, W01410, doi:10.1029/2005WR004233.
- Gao, B., T. S. Steenhuis, Y. Zevi, V. L. Morales, J. L. Nieber, B. K. Richards, J. F. McCarthy, and J.-Y. Parlange (2008), Capillary retention of colloids in unsaturated porous media, *Water Resour. Res.*, *44*, W04504, doi:10.1029/2006WR005332.
- Ghosh, J. C., and M. C. Nath (1932), The variation of the surface tension of aqueous solutions of certain complex organic substances with time, *J. Phys. Chem.*, *36*(7), 1916–1927, doi:10.1021/j150337a005.
- Jewett, D. G., B. E. Logan, R. G. Arnold, and R. C. Bales (1995), Bacterial transport in laboratory columns and filters: influence of ionic strength and pH on collision efficiency, *Water Res.*, *29*, 1673–1680, doi:10.1016/0043-1354(94)00338-8.
- Johnson, R. P. (1999), A comparison of streaming and microelectrophoresis methods for obtaining the ζ potential of granular porous media surfaces, *J. Colloid Interface Sci.*, *209*(1), 264–267, doi:10.1006/jcis.1998.5908.
- Kralchevsky, P. A., and K. Nagayama (2000), Capillary interactions between particles bound to interfaces, liquid films and biomembranes, *Adv. Colloid Interface Sci.*, *85*, 145, doi:10.1016/S0001-8686(99)00016-0.
- Kralchevsky, P. A., N. D. Denkov, and K. D. Danov (2001), Particles with an undulated contact line at a fluid interface: Interaction between capillary quadrupoles and rheology of particulate monolayers, *Langmuir*, *17*, 7694–7705, doi:10.1021/la0109359.
- Kretzschmar, R., and H. Sticher (1998), Colloid transport in natural porous media: Influence of surface chemistry and flow velocity, *Phys. Chem. Earth*, *23*, 133–139, doi:10.1016/S0079-1946(98)00003-2.
- Lazouskaya, V., and Y. Jin (2008), Colloid retention at air-water interface in a capillary channel, *Colloids Surf. A*, *325*, 141–151, doi:10.1016/j.colsurfa.2008.04.053.
- Lazouskaya, V., Y. Jin, and D. Or (2006), Interfacial interactions and colloid retention under steady flows in a capillary channel, *J. Colloid Interface Sci.*, *303*, 171, doi:10.1016/j.jcis.2006.07.071.
- Lenhart, J., and J. Saiers (2002), Transport of silica colloids through unsaturated porous media: Experimental results and model comparisons, *Environ. Sci. Technol.*, *36*(4), 769–777, doi:10.1021/es0109949.
- Li, Q., and B. E. Logan (1999), Enhancing bacterial transport for bioaugmentation of aquifers using low ionic strength solutions and surfactants, *Water Res.*, *33*(4), 1090–1100, doi:10.1016/S0043-1354(98)00291-7.
- Li, Z. B., Y.-G. Li, and J.-F. Lu (1999), Surface tension model for concentrated electrolyte aqueous solutions by the Pitzer equation, *Ind. Eng. Chem. Res.*, *38*, 1133–1139, doi:10.1021/ie980465m.
- Morales, V. L., B. Gao, and T. S. Steenhuis (2009), Grain surface-roughness effects on colloidal retention in the vadose zone, *Vadose Zone J.*, *8*, 11–20, doi:10.2136/vzj2007.0171.
- Ouyang, Y., D. Shinde, R. S. Mansell, and W. Harris (1996), Colloid-enhanced transport of chemicals in subsurface environments: A review, *Crit. Rev. Environ. Sci. Technol.*, *26*, 189–204, doi:10.1080/10643389609388490.
- Poling, B. E., J. M. Prausnitz, and J. P. O'Connell (Eds.) (2001), *The Properties of Gases and Liquids*, McGraw-Hill, New York.
- Saiers, J. E., and J. J. Lenhart (2003), Ionic-strength effects on colloid transport and interfacial reactions in partially saturated porous media, *Water Resour. Res.*, *39*(9), 1256, doi:10.1029/2002WR001887.
- Schäfer, A., P. Ustohal, H. Harms, F. Stauffer, T. Dracos, and A. J. B. Zehnder (1998a), Transport of bacteria in unsaturated porous media, *J. Contam. Hydrol.*, *33*, 149–169, doi:10.1016/S0169-7722(98)00069-2.

- Schäfer, A., H. Harms, and A. J. B. Zehnder (1998b), Bacterial accumulation at the air-water interface, *Environ. Sci. Technol.*, *32*(23), 3704–3712, doi:10.1021/es980191u.
- Sen, T. K., and K. C. Khilar (2006), Review on subsurface colloids and colloid-associated contaminant transport in saturated porous media, *Adv. Colloid Interface Sci.*, *119*, 71–96, doi:10.1016/j.cis.2005.09.001.
- Shang, J., M. Flury, G. Chen, and J. Zhuang (2008), Impact of flow rate, water content, and capillary forces on in situ colloid mobilization during infiltration in unsaturated sediments, *Water Resour. Res.*, *44*, W06411, doi:10.1029/2007WR006516.
- Shang, J., M. Flury, and Y. Deng (2009), Force measurements between particles and the air-water interface: Implications for particle mobilization in unsaturated porous media, *Water Resour. Res.*, *45*, W06420, doi:10.1029/2008WR007384.
- Sirivithayapakorn, S., and A. Keller (2003), Transport of colloids in unsaturated porous media: A pore-scale observation of processes during the dissolution of air-water interface, *Water Resour. Res.*, *39*(12), 1346, doi:10.1029/2003WR002487.
- Sur, J., and H. K. Pak (2001), Capillary force on colloidal particles in a freely suspended liquid thin film, *Phys. Rev. Lett.*, *86*, 4326–4329, doi:10.1103/PhysRevLett.86.4326.
- Tong, M., H. Ma, and W. P. Johnson (2008), Funneling of flow into grain-to-grain contacts drives colloid colloid aggregation in the presence of an energy barrier, *Environ. Sci. Technol.*, *42*, 2826–2832.
- Torkzaban, S., S. A. Bradford, and S. L. Walker (2007), Resolving the coupled effects of hydrodynamics and DLVO forces on colloid attachment to porous media, *Langmuir*, *23*, 9652–9660, doi:10.1021/la700995e.
- Torkzaban, S., S. S. Tazehkand, S. L. Walker, and S. A. Bradford (2008), Transport and fate of bacteria in porous media: Coupled effects of chemical conditions and pore space geometry, *Water Resour. Res.*, *44*, W04403, doi:10.1029/2007WR006541.
- Wan, J., and T. Tokunaga (1997), Film straining of colloids in unsaturated porous media: Conceptual model and experimental testing, *Environ. Sci. Technol.*, *31*, 2413–2420, doi:10.1021/es970017q.
- Wan, J., and J. L. Wilson (1994a), Colloid transport in unsaturated porous media, *Water Resour. Res.*, *30*(4), 857–864, doi:10.1029/93WR03017.
- Wan, J., and J. L. Wilson (1994b), Visualization of the role of the gas-water interface on the fate and transport of colloids in porous media, *Water Resour. Res.*, *30*(1), 11–23, doi:10.1029/93WR02403.
- Weisbrod, N., R. M. Niemet, and J. S. Selker (2003), Light transmission technique for the evaluation of colloidal transport and dynamics in porous media, *Environ. Sci. Technol.*, *37*, 3694–3700, doi:10.1021/es034010m.
- Zevi, Y., A. Dathe, J. F. McCarthy, B. K. Richards, and T. S. Steenhuis (2005), Distribution of colloid particles onto interfaces in partially saturated sand, *Environ. Sci. Technol.*, *39*(18), 7055–7064, doi:10.1021/es048595b.
- Zevi, Y., A. Dathe, B. Gao, B. K. Richards, and T. S. Steenhuis (2006), Quantifying colloid retention in partially saturated porous media, *Water Resour. Res.*, *42*, W12S03, doi:10.1029/2006WR004929.

A. Dathe, B. K. Richards, T. S. Steenhuis, Y. Zevi, and W. Zhang, Department of Biological and Environmental Engineering, Cornell University, Riley-Robb Hall, Ithaca, NY 14853-5701, USA. (tss1@cornell.edu)

B. Gao, Department of Agricultural and Biological Engineering, University of Florida, Gainesville, FL 32611, USA.